

Density Functional Study of the $L1_0$ - α IrV Transition in IrV and RhV

Michael J. Mehl

*Center for Computational Materials Science, Naval Research Laboratory, Code 6390,
Washington DC 20375-5000, USA*

Gus L. W. Hart

*Department of Physics and Astronomy, Brigham Young University, Provo, UT 84602,
USA*

Stefano Curtarolo

*Department of Mechanical Engineering and Materials Science and Department of
Physics, Duke University, Durham NC 27708, USA*

Abstract

Both IrV and RhV crystallize in the α IrV structure, with a transition to the higher symmetry $L1_0$ structure at high temperature, or with the addition of excess Ir or Rh. Here we present evidence that this transition is driven by the lowering of the electronic density of states at the Fermi level of the α IrV structure. The transition has long been thought to be second order, with a simple doubling of the $L1_0$ unit cell due to an unstable phonon at the R point ($0\frac{1}{2}\frac{1}{2}$). We use first-principles calculations to show that all phonons at the R point are, in fact, stable, but do find a region of reciprocal space where the $L1_0$ structure has unstable (imaginary frequency) phonons. We use the frozen phonon method to examine two of these modes, relaxing the structures associated with the unstable phonon modes to obtain new structures which are lower in energy than $L1_0$ but still above α IrV. We examine the phonon spectra of these structures as well, looking for instabilities, and find further instabilities, and more relaxed structures, all of which have energies above the α IrV phase. In addition, we find that all of the relaxed structures, stable

Email address: Michael.Mehl@nr1.navy.mil (Michael J. Mehl)

and unstable, have a density comparable to the $L1_0$ phase (and less than the αIrV phase), so that any transition from one of these structures to the ground state will have a volume change as well as an energy discontinuity. We conclude that the transition from $L1_0$ to αIrV is probably weakly first order.

Keywords: Structural Phase Transitions, Jahn-Teller, Electronic Structure, Density Functional Theory, Ordered Intermetallic Alloys,

1. Introduction

A major goal of computational condensed matter physics is the determination of structural properties for compounds. Once the structure has been determined, other properties, e.g., strength, ductility, electronic properties (including superconductivity), magnetism, etc., can be determined. Several methods exist to attack this problem. One possibility is to exhaustively search an experimental database of known structures[1], determining the low energy structures for each composition of the target materials. Other methods use first-principles calculations on a small set of target structures to determine parameters which can be used to predict properties of more complex systems. These include the Cluster Expansion Method[2, 3, 4, 5, 6], tight-binding parametrization methods[7, 8], and atomistic potential methods[9]. Methods of the first type can be combined with methods of the second type for more thorough searches[10].

These programs, can, however, only be implemented with a thorough knowledge of the behavior of compounds. Exhaustive searches of a database require an extensive database to search, including all structures which are known, or thought likely, to form for a target system. Parameterized methods may not be able to reach all regions of phase space, and also need a database of structures for testing[11, 12]. For both methods, then, it is useful to look at less-common structures found in nature.

The αIrV structure, shown in Figure 1, is found in nature only in the prototype compound[13, 14] and its neighbor in the periodic table, RhV [15, 16]. This orthorhombic structure, space group Cmmm (#65), can be viewed as a doubled unit cell distortion of the CsCl structure[17] or the tetragonal $L1_0$ structure, space group P4/mmm (#123)[18]. Indeed, both the IrV and RhV phase diagrams[19] show the $L1_0$ structure as the ground state for Vanadium-poor ($x = 40 - 48\%$) $[\text{Ir,Rh}]_{1-x}\text{V}_x$, and Vanadium-rich αIrV is known to

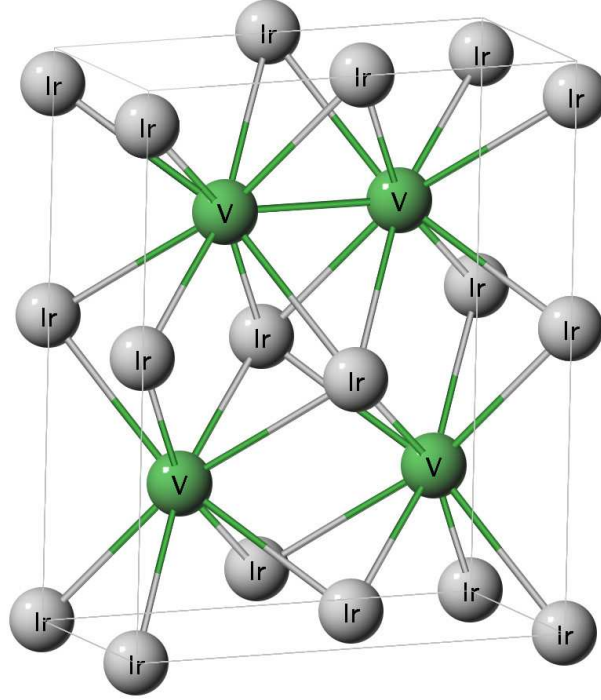


Figure 1: The α IrV structure. The box indicates the boundaries of the full orthorhombic unit cell. In the $L1_0$ or (CsCl) structure the Iridium atoms would be in a tetragonal (cubic) arrangement around each of the Vanadium atoms.

transform to $L1_0$ at temperatures above 506°C [18].

The seemingly straightforward transition pathway from $L1_0$ to α IrV was analyzed by Chen and Franzen[18] in the context of Landau theory: First, double the tetragonal $L1_0$ unit cell along the y and z directions, corresponding to a phonon at the R $(0\frac{1}{2}\frac{1}{2})$ point in reciprocal space. Second, construct the primitive base-centered orthogonal unit cell, and allow the two Ir atoms in the cell to move opposite each other along the z -axis, while the V atoms move along the y -axis. The resulting structure is symmetrically-equivalent to that of α IrV and, assuming a second-order phase transition, relaxes into the α IrV structure.

This simple picture is not quite accurate. A true second order transition, as described by Chen and Franzen, requires a continuous energy path from $L1_0$ to α IrV. Thus the energy of the $L1_0$ structure would be lowered

by making an infinitesimal displacement of the type described above, corresponding to a phonon instability at the R point. We have performed first-principles density functional theory calculations for the phonon frequencies at the R point, both by the frozen phonon method[20] and by linear response[21, 22, 23]. We find that all of the modes here have real frequencies, i.e., they do not lead to an instability.

Thus the transition from the L1₀ phase to the α IrV phase does not proceed through the simple unit-cell doubling picture described above. Instead, as we shall show, the L1₀ phase has vibrational instabilities in another region of the Brillouin zone. This paper will discuss the structures arising from these instabilities, and explore the possibility that a second-order transition might go through one of those phases.

In Section 2 we show the results of density functional theory calculations for the energy and electronic structure of the α IrV and L1₀ phases of IrV, RhV, and some neighboring compounds. We show that in IrV and RhV the L1₀ structure has a relatively high electronic density of states at the Fermi level, and so the transition to α IrV has Jahn-Teller character[24].

In Section 3 we look at the phonon spectra of the α IrV and L1₀ phase. Not surprisingly, we find that the α IrV phase has no phonon instabilities. We do, however, find that the L1₀ structure is vibrationally unstable on and near the line $(x\frac{1}{4}\frac{1}{2})$ in reciprocal space.

In Section 4 we use the frozen-phonon method on the unstable phonon modes to search for new structures which have lower energy than L1₀. Such a search is computationally bound, so we looked at all unit cells with eight atoms or less, and two structures with 32 atom unit cells. In this range we find no instability which relaxes to the α IrV phase, however it is not impossible that searching through larger unit cells would find such an instability, in which case the transition would indeed be second order. We do find several new structures, some of which have apparently never been seen in nature, and one which was previously known[16].

In Section 5 we discuss our results, and thoughts on the order of the L1₀- α IrV transition.

2. Energetics and Electronic Structure of the L1₀ and α IrV Phases

All computations were made using the Kohn-Sham[25] formulation of Density Functional Theory[26] with the Perdew-Burke-Ernzerhof[27] generalized gradient approximation. Depending on our needs, we used the Vienna

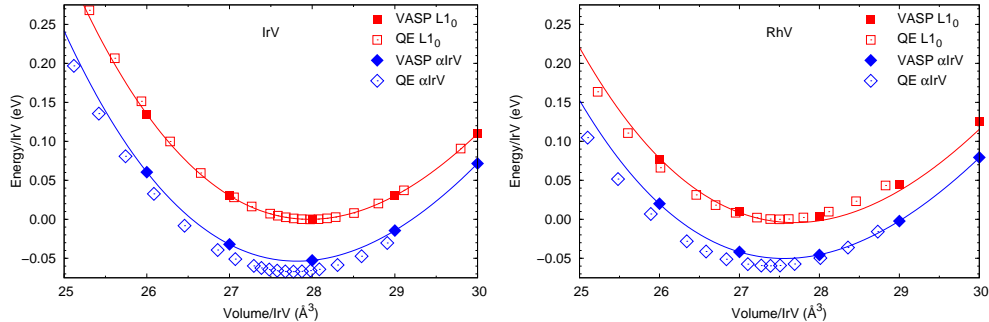


Figure 2: Energy/volume curves for IrV and RhV in the $L1_0$ and α IrV structures, determined from VASP and QE calculations as discussed in the text. For ease of comparison we have set the minimum energy of the $L1_0$ phase to zero.

ab initio Simulation Package (VASP)[28, 29, 30] with projector augmented-wave (PAW) potentials[31], or the *Quantum Espresso* (QE) package[32] with the supplied ultra-soft pseudopotentials for Ir, Rh, and V.

We used rather large plane wave cutoffs of 350 eV in VASP and 540 eV in QE to ensure convergence. Similarly, we used $12 \times 12 \times 8$ Γ -centered k-point meshes in both the $L1_0$ and α IrV structures, leading to 140 and 215 points, respectively, in the irreducible Brillouin zones. We summed over electronic states using a Fermi-Dirac distribution[33] with a temperature of 65 meV (0.005 Rydbergs). These values give well-converged results.

We show our results for IrV and RhV in Table 1 and Fig. 2. In both cases we see that the VASP PAW potentials and the QE ultrasoft pseudopotentials are in excellent agreement with one another, and in good agreement with experiment, within the usual errors of Density Functional theory in the generalized gradient approximation. In both compounds the α IrV state is below the $L1_0$ state by approximately 55 meV/formula unit, in agreement with experiment.

From experiment[18] we know that $L1_0$ is the preferred high temperature structure for α IrV. Using the COMSUBS routine from the ISOTROPY[34, 35] package, we find that an orthorhombic distortion of the $L1_0$ structure reduces the symmetry from space group $P4/mmm$ to $Cmmm$, the space group of the α IrV structure. It is plausible to argue[18] that this lowering of symmetry is the pathway for the $L1_0 \rightarrow \alpha$ IrV phase transition. The symmetry-breaking character of the transition is evident from Fig. 3, where we plot the electronic density of states of both phases near the Fermi level.

Table 1: Equilibrium lattice constants (in Å), atomic positions, and equilibrium bulk modulus (K_0 , in GPa) for the $L1_0$ and α IrV structures of IrV and RhV determined from experiment[13, 15], VASP PAW calculations, and QE ultrasoft pseudopotential calculations. Note that we give the primitive tetragonal lattice parameters for the $L1_0$ structure, rather than the more-common face-centered tetragonal setting, so that when $c/a = 1$ the $L1_0$ structure reduces to the cubic CsCl structure. The final row of the table shows the energy difference between the two phases (meV/formula unit).

	IrV			RhV		
$L1_0$ Structure						
	Exp.	VASP	QE	Exp.	VASP	QE
a	2.749	2.755	2.762	2.754	2.739	2.745
c	3.651	3.677	3.668	3.599	3.660	3.648
K_0		272	277		230	
α IrV Structure						
a	5.791	5.838	5.816	5.78	5.849	5.813
b	6.756	6.759	6.767	6.65	6.707	6.725
c	2.796	2.814	2.823	2.78	2.792	2.802
K_0		271	276	227		
Ir/Rh (4j)	0.22	0.216	0.216		0.214	0.215
V (4g)	0.28	0.296	0.297		0.296	0.297
ΔE						
		53.6	67.0		50.4	59.7

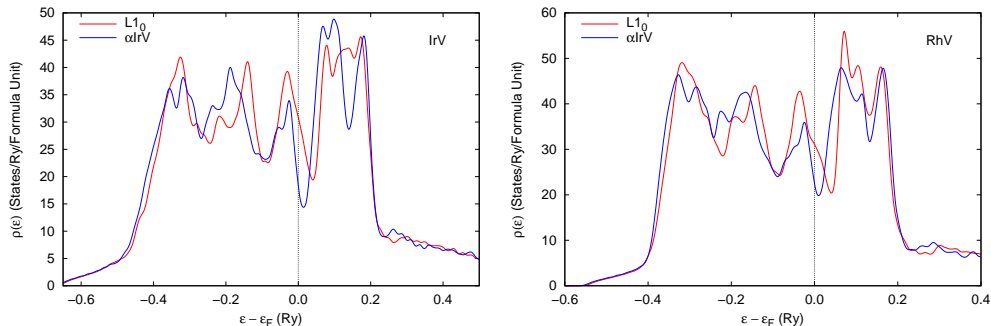


Figure 3: Electronic density of states for the $L1_0$ (red) and αIrV (blue) phases of IrV (left) and RhV (right), found by smearing the eigenvalues computed by VASP using a Fermi-Dirac distribution at $T = 65$ meV (5 mRY).[33]

As we are only interested in the overall behavior of the density of states, we compute these curves by smearing out each eigenvalue found by VASP using a Fermi distribution at a temperature of 5 mRy. We see that at the Fermi level the density of states is twice as large in the $L1_0$ phase as it is in the αIrV phase. This is consistent with a Jahn-Teller-like symmetry breaking and phase transition[24]. As an aside, we also note that there is a minimum in the $L1_0$ density of states just above the Fermi level. This is consistent with the phase diagram of IrV[19], which shows that Iridium-rich IrV has the $L1_0$ structure. Assuming the additional Ir replaces V in the $L1_0$ structure, and using a rigid-band model, we can see how adding Ir to the system would raise the Fermi level and lower the density of states, leading to a more stable $L1_0$ phase. We find a similar, though less pronounced, state of affairs in RhV, as is also seen in Fig. 3.

We investigated the possibility that the αIrV structure might be found in compounds neighboring IrV and RhV in the periodic table. The results are shown in Table 2. Except for CoPt, all of the compounds shown here have 14 electrons in the valence band, just as in IrV and RhV. In all cases except CoPt we found that the αIrV structure was locally stable, that is, if we started from the lattice parameters of the αIrV , replacing Ir and V by the indicated atoms, and allowed the system to relax, it remained in the αIrV structure and did not relax to the higher symmetry $L1_0$ structure. This suggests that the formation of the αIrV structure is a result of a Fermi level effect associated with 14 electrons in a tetragonal unit cell. We did not check the elastic and vibrational stability of the resulting structure. However the

Table 2: Energy difference, in meV per formula unit between the $L1_0$ and α IrV structures for the given compounds, as determined by VASP/PAW/PBE calculations. A positive number indicates that the $L1_0$ structure is lower in energy. An energy difference of zero indicates that the α IrV structure relaxes into the $L1_0$ structure. Ground state structures are from the *ASM Online Handbook*[19].

Compound	CoPt	CoV	IrNb	IrTa	IrV	RhNb	RhTa	RhV
Ground State	$L1_0$	$D8_b$	$L1_0$		α IrV	$L1_0$		α IrV
ΔE	0	25.3	59.0	79.9	-53.6	50.1	70.6	-50.4

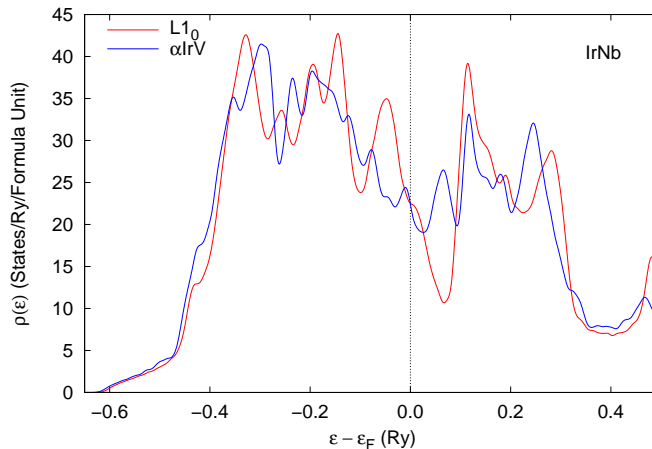


Figure 4: Electronic density of states of the ground-state $L1_0$ and hypothetical α IrV phases of IrNb, found by smearing the eigenvalues computed by VASP.

$L1_0$ structure was lower in energy for all compounds except IrV and RhV. Also, as shown in Fig. 4, for these compounds the density of states of the $L1_0$ structure is very near to that of the α IrV structure, precluding a Jahn-Teller lowering of the energy with decreased symmetry. We therefore conclude that it is unlikely to find the α IrV structure anywhere except in IrV and RhV.

3. Stability of the $L1_0$ and α IrV Phases

A system is stable, or metastable, only if it has real phonon frequencies for all k-points and modes except the acoustic phonons at the Γ point, which are guaranteed to vanish because of translational symmetry. Since the elastic constants are related to the long-wavelength behavior of the acoustic phonons[37] this implicitly includes the Born stability criteria[38]. This is for-

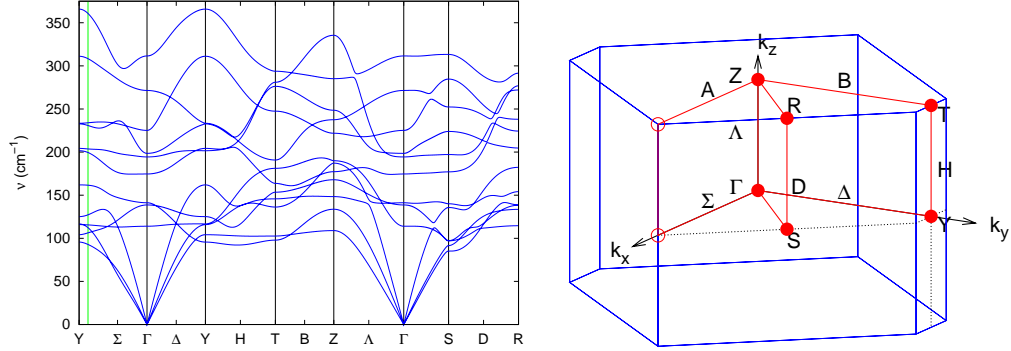


Figure 5: The base-centered orthorhombic α IrV structure. Left: Phonon frequencies IrV at equilibrium, determined using the linear response method with ultrasoft pseudopotentials from the *Quantum Espresso* package. Right: First Brillouin zone. Symmetry lines are described by the notation of Miller and Love[36].

tunate, since the orthorhombic α IrV structure would require us to compute nine elastic constants.

To check the stability of the α IrV phase and the possible meta-stability of the $L1_0$ phase we computed phonon frequencies throughout the respective Brillouin zones using linear response[21, 22, 23], as implemented in the *Quantum Espresso* package PHon code[32]. Phonon frequencies were computed on a reciprocal space grid (“q-points”) using an $8 \times 8 \times 4$ mesh for the $L1_0$ structure (45 points in the irreducible Brillouin zone) and a $6 \times 6 \times 4$ mesh for the α IrV structure (39 points). Linear response calculations at these points yield a reciprocal-space dynamical matrix. These matrices are transformed into a real-space dynamical matrix which can be used to compute phonon frequencies over the entire Brillouin zone.

This approach can lead to aliasing at points off of the q-point mesh. To check that this does not occur we also performed frozen-phonon calculations[20], wherein we construct a supercell commensurate with the given q-point and measure the change in energy as a function of atomic displacement within the supercell. To do this we used the program FROZSL, part of the ISOTROPY package[34, 35], with atomic displacements of 0.1 Bohr. Electronic structure calculations were then performed with the same energy cutoff as the original unit cell, and when possible the same k-point mesh, albeit folded back into the smaller Brillouin zone associated with the supercell.

In the following, in interest of saving space, we only show the results for

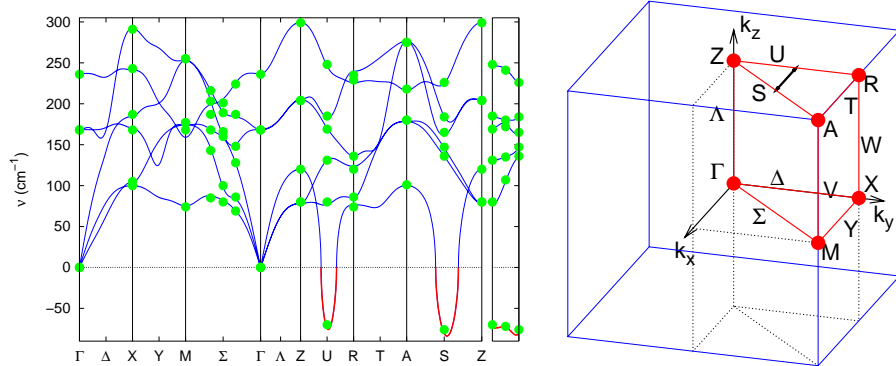


Figure 6: The tetragonal $L1_0$ structure. Left: Phonon frequencies for IrV at its minimum energy structure, determined using the linear response method, using ultrasoft pseudopotentials from the *Quantum Espresso* package. Frequencies below zero (and in red) are unstable modes which actually have imaginary frequencies. The dots represent calculations using the frozen phonon method with displacements computed by FROZSL. The second panel shows the frequencies along the line $(x\frac{1}{4}\frac{1}{2})$. Right: First Brillouin zone, with symmetry lines labeled according to the notation of Miller and Love[36]. The arrow from U to S indicates the region of unstable phonons.

IrV. Our calculations for RhV show a similar pattern.

Fig. 5 shows the phonon frequencies of the equilibrium structure of α IrV. High symmetry points and lines are labeled according to the convention of Miller and Love[36]. All the phonons have real frequencies, confirming that α IrV is at least a metastable structure for IrV, as suspected. There is no evidence of any aliasing in these calculations.

Figure 6 shows the phonon frequencies of the $L1_0$ phase of IrV, along symmetry lines labeled according to the convention of Miller and Love[36]. We show results of frozen phonon calculations, showing good agreement between the two techniques, even off the linear response q-mesh. As expected, there are regions of reciprocal space with imaginary phonon frequencies. Surprisingly, this region is not near the R point $(0\frac{1}{2}\frac{1}{2})$ as described by Chen and Franzen[18], but along and near a line from the midpoint of the U line to the midpoint of the S line, as shown in more detail in the second panel of the figure. We will discuss the implications of this instability in the next section.

4. Searching for Low Energy Structures

The previous section showed that the α IrV structure is the ground state (or, at least, a low-energy metastable state) of IrV, while the $L1_0$ structure is

unstable to phonons along and near the line $(x\frac{1}{4}\frac{1}{2})$ in the Brillouin zone, but not at the R point, where the phonon modes are real, invalidating the second-order phase transition scenario of Chen and Franzen[18]. In this section we will look to see if it is possible to find another continuous transition path from $L1_0$ to αIrV .

In the frozen phonon method, we displace atoms from their equilibrium sites in a supercell consistent with the phonon wave vector and in directions which maintain the symmetry of the phonon mode. The frequency of the mode is then directly related to the square root of the curvature of the energy as a function of atom displacement. A mode with an imaginary frequency will then as a matter of course be related to a supercell calculation which has a negative curvature, leading to supercells with energy lower than the original state. These structures can then be relaxed, leading to new, or at least different, structures.

As an example of this, consider the unstable $L1_0$ phonon at the point $(\frac{1}{4}\frac{1}{4}\frac{1}{2})$ on the high symmetry ‘‘S’’ line. The linear response calculations find this phonon frequency to be $81i\text{ cm}^{-1}$. To generate a supercell for this calculation we used the FROZSL code from the ISOTROPY package[34, 35]. This package tells us that this point has phonons in three irreducible representations, each with two associated modes. For each representation we run three total energy calculations for displacements of the atoms in different directions, with the maximum displacement of 0.1 Bohr. The energy differences between these structures and the ground state are used to determine the dynamical matrix at this point, and the mode frequencies.

For the equilibrium $L1_0$ parameters found in Table 1, the S_3 irreducible representation (in the notation of Miller and Love[36]) has one mode with an imaginary frequency of 74 cm^{-1} . (The discrepancy between linear response and frozen phonon calculations is due to the use of different k-point meshes and the anharmonicity of the mode. For our purposes we are only interested in showing that the mode is unstable in both cases, and so will not try to refine the calculations to improve the agreement between the two.)

Diagonalizing the dynamical matrix allows us to find a supercell with displaced atoms which has an energy lower than the $L1_0$ phase. This supercell has space group Cmmm (#65), and with the appropriate choice of origin has Ir atoms at the (4e) and (4h) Wyckoff positions, and V atoms at the (2a), (2b), and (4j) positions. This is crystallographically equivalent to the intermetallic Ga_3Pt_5 structure [39], and we will refer to it as such. Upon relaxation we find a minimum energy structure which has approximately the

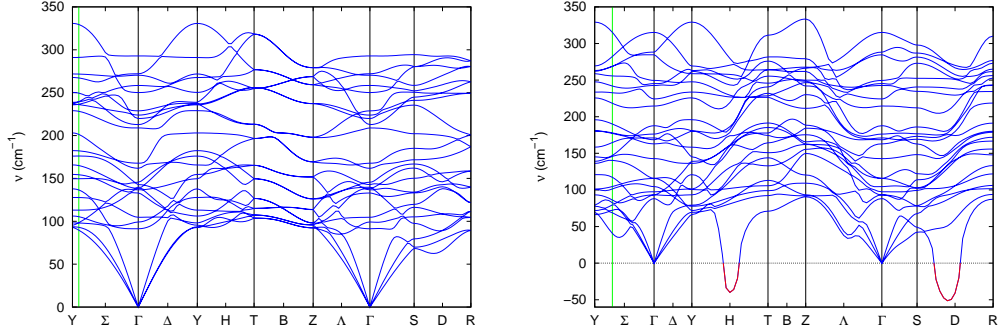


Figure 7: Linear-response phonon spectra of two eight-atom unit cells derived from unstable phonon modes of $L1_0$ IrV. Left: The metastable Rh_5V_3 structure. Right: The $Amm2$ structure with Ir atoms at two (4d) Wyckoff positions and V atoms at four (2b) Wyckoff positions. The imaginary frequencies of the unstable modes are shown as negative frequencies and highlighted in red.

same density as, and an energy 20.5 meV/formula unit below, the relaxed $L1_0$ structure of Table 1. Note that this is still well above the energy of the α IrV structure.

In a similar fashion, if we look at the phonons at $0\frac{1}{4}\frac{1}{2}$, on the “U” line, we find an imaginary U_3 mode with a frequency of 70 cm^{-1} . This mode leads to another supercell with space group $Cmmm$, but now the Ir atoms are on the (4e) and (4g) Wyckoff sites, while the V atoms occupy a pair of (4j) Wyckoff sites. The relaxed structure again has a density comparable to $L1_0$, but its energy is only 11.0 meV/formula unit below the $L1_0$ structure minimum. In the discussion below will refer to this structure as $Cmmm$.

Neither the Ga_3Pt_5 nor the $Cmmm$ structure will relax to the ground state α IrV structure. However, both structures have imaginary frequency long-wavelength optical mode phonons. If we venture away from the Γ point we will have to deal with frozen-phonon calculations on unit cells having hundreds of atoms, so we will only examine the unstable modes at Γ in both structures.

First consider the imaginary frequency Γ_4^- mode of the Ga_3Pt_5 structure. It is associated with a supercell of space group $Amm2$ (#38), with Ir atoms at the (4d) and (4e) Wyckoff sites and V atoms on pairs of (2a) and (2b) sites. This structure is crystallographically equivalent to the Rh_5V_3 structure[16, 40] and will be referred to by that name. The relaxed structure is 41.1 meV/formula unit below the $L1_0$ structure, with similar density.

This structure is metastable, as seen in the linear-response phonon spectrum plotted on the left-hand side of Fig. 7.

The second structure, derived from the unstable Γ_3^- mode of Cmmm, again with space group Amm2 (#38), puts the Ir atoms on two (4d) sites and the V atoms on four distinct (2b) sites. The relaxed structure has an energy 24.1 meV/formula unit below the L1₀ structure, again with a similar density. This structure has not been found in the intermetallic literature. It is vibrationally unstable, as can be seen from the phonon spectrum on the right-hand side of Fig. 7.

The four structures Ga₃Pt₅, Rh₅V₃, Cmmm and Amm2 are the only structures with eight or fewer atoms in the primitive cell which can be generated by relaxing the unstable phonon modes of the L1₀ structure. If we wish to examine larger unit cells, we can continue along this line of research *ad infinitum*, or until we find a supercell where the atoms relax to the ground state α IrV structure, a supercell with energy *below* the ground state structure, or we run out of computational resources. In most cases, including this one, we will reach the latter limit first. We did compute the relaxed energies of two supercells associated with unstable phonon modes in the Amm2 structure, and one with an unstable mode of the Cmmm structure. These structures had thirty-two atoms in the supercell, and energies below the parent structure but above the metastable Rh₅V₃ structure.

Tables 3, 4 and 5 summarize all of the calculations discussed here, including the structural derivation, space group, lattice constants, atomic positions, energy, and stability.

5. Discussion

We have shown by direct calculation that the transition from the L1₀ to the α IrV structure of both IrV and RhV is a result of a Jahn-Teller driven distortion of the high-symmetry unit cell. This distortion does not result from a zone-doubling unstable phonon at the R point of the L1₀ Brillouin zone, and so the simple Landau theory picture does not hold. This does not completely eliminate the possibility that the transition is second order, for we found an entire region of reciprocal space, in and around the line $(x\frac{1}{4}\frac{1}{2})$, where the L1₀ structure has vibrational instabilities. We examined several of those instabilities, and found that they lead to numerous new structures, most of which have yet to be seen in ordered intermetallic systems and most of which are vibrationally unstable. The only phase which we found that

Table 3: Structural, energy, and vibrational stability results for the structures of IrV discussed in this paper. All calculations use the QE pseudopotentials discussed in the text. “Source” indicates the origin of the unit cell, either from experiment or an unstable phonon in the indicated structure. “Atoms” is the number of atoms in the primitive cell. Lattice constants are given in the standard crystallographic convention, e.g. the lattice constants of the full orthorhombic cell are given for the Cmmm and Cmcmm space groups. All primitive cells have $\alpha = \gamma = 90^\circ$. The rows “Ir” and “V” give the Wyckoff positions of the atoms. “Volume” is the minimum energy volume of the structure per formula unit, in (\AA^3). “Energy” is the energy of the structure below the L1₀ structure, in meV/formula unit.

Structure	L1 ₀	Cmmm	Cmcmm
Source	Exp.	U ₃ (0 $\frac{1}{4}$ $\frac{1}{2}$) L1 ₀ phonon	Λ_3 (00 $\frac{1}{4}$) Cmmm phonon
Space Group	P4/mmm	Cmmm	Cmcmm
Atoms	2	8	32
a (\AA)	2.762	7.260	7.198
b (\AA)	2.762	11.110	11.166
c (\AA)	3.668	2.774	11.136
β	90	90	90
Ir	(1a) (000)	(4e)($\frac{1}{4}\frac{1}{4}0$) (4g)(.267 0 0)	(4d)($\frac{1}{4}\frac{1}{4}0$) (4e)(.269 0 0) (4g)(.273 .254 $\frac{1}{4}$) (4g)(.268 .002 $\frac{1}{4}$)
V	(1d) ($\frac{1}{2}\frac{1}{2}0$)	(4j)(0 .364 $\frac{1}{2}$) (4j)(0 .115 $\frac{1}{2}$)	(4f)(0 .358 .134) (4f)(0 .632 .117) (4f)(0 .123 .132) (4f)(0 .895 .117)
Volume	27.97	27.97	27.97
Energy	0	10.98	20.61
Stability	Unstable	Unstable	Unknown

Table 4: Continuation of Table 3.

Structure	Ga_3Pt_5	Amm2	Imm2
Source	$\text{S}_3(\frac{1}{4}\frac{1}{4}\frac{1}{2})$ L1 ₀ phonon	Γ_3^- Cmmm phonon	$\text{H}_1(\frac{1}{4}00)$ Amm2 phonon
Space Group	Cmmm	Amm2	Imm2
Atoms	8	8	32
a (Å)	7.222	2.788	7.176
b (Å)	7.800	7.146	11.144
c (Å)	3.974	11.230	11.190
β	90	90	90
Ir	(4e)($\frac{1}{4}\frac{1}{4}0$) (4h)(.273 0 $\frac{1}{2}$)	(4d)(0 .230 .752) (4d)(0 .270 .998)	(4c)(.256 0 .252) (8e)(.268 2.50 .252) (4c)(0.223 0 .752) (4c)(.256 0 .998) (8e)(.268 .250 .998) (4c)(.223 0 .498)
V	(2a)(000) (2b)($\frac{1}{2}\frac{1}{2}0$) (4j) (0 .218 $\frac{1}{2}$)	(2b)($\frac{1}{2}$ 0 .352) (2b)($\frac{1}{2}$ 0 .625) (2b)($\frac{1}{2}$ 0 .125) (2b)($\frac{1}{2}$ 0 .899)	(4d)(0 .131 .352) (4d)(0 .381 .355) (4d)(0 .132 .625) (4d)(0 .384 .625) (4d)(0 .130 .125) (4d)(0 .380 .125) (4d)(0 .131 .898) (4d)(0 .381 .895)
Volume	27.98	27.97	27.96
Energy	20.25	24.15	25.12
Stability	Unstable	Unstable	Unknown

Table 5: Continuation of Tables 3 and 4.

Structure	Cm	Rh ₅ V ₃	α IrV
Source	$\Delta_1(0\frac{1}{4}0)$ Amm2 phonon	Γ_4^- Ga ₃ Pt ₅ phonon	Exp.
Space Group	Cm	Amm2	Cmmm
Atoms	32	8	4
a (Å)	13.303	4.070	5.816
b (Å)	11.147	7.029	6.767
c (Å)	6.652	7.822	2.823
β	65.3	90	90
Ir	(2a)(.999 0 .504) (2a)(.265 0 .974) (2a)(.485 0 .534) (2a)(.755 0 .994) (2a)(.870 0 .256) (2a)(.140 0 .715) (2a)(.360 0 .276) (2a)(.626 0 .745) (4b)(.992 .249 .521) (4b)(.260 .252 .983) (4b)(.365 .748 .267) (4b)(.133 .251 .729)	(4d)(0 .219 .724) (4e)($\frac{1}{2}$.281 .001)	(4j)(0 .216 $\frac{1}{2}$)
V	(4b)(.178 .130 .344) (4b)(.175 .380 .362) (4b)(.312 .134 .625) (4b)(.312 .385 .625) (4b)(.064 .125 .117) (4b)(.060 .375 .133) (4b)(.447 .130 .906) (4b)(.450 .380 .888)	(2a)(0 0 .032) (2a)(0 0 .457) (2b)($\frac{1}{2}$ 0 .218) (2b)($\frac{1}{2}$ 0 .793)	(4g)(.297 0 0)
Volume	27.97	27.97	27.78
Energy	25.67	41.14	67.25
Stability	Unknown	Metastable	Ground State

is metastable is the experimentally observed Rh_5V_3 phase, albeit in a 50-50 composition.

However, none of the unstable structures shows any sign of relaxing into the ground state structure. In fact, looking at Tables 3-5, we see that all of the structures except αIrV have approximately the same volume, $27.97 \text{ \AA}^3/\text{formula unit}$ in IrV . The ground state αIrV structure, on the other hand, has a somewhat smaller volume, $27.78 \text{ \AA}^3/\text{formula unit}$. While this may seem insignificant, the volume change from one phase to another is a signal of a first-order transition, although only weakly first order here.

This paper also shows a mechanism for generating new candidate intermetallic phases: look for vibrationally unstable modes in a high energy structure, construct a supercell which will mimic that mode within the frozen-phonon calculation, and relax the cell. Using this method we found five new structures, as well as one, Rh_5V_3 , which had been seen before but which we had not been aware of until this research started. Many more new structures can undoubtedly be derived from just this system, but further research in this area is currently restricted by the time needed to search the Brillouin zone of a given crystal. For the eight atom supercells computing the phonon spectrum at 45 q-points with a reasonable number (≤ 64) of processors took days to weeks to complete, depending on the symmetry of the crystal. Calculating the phonons for larger unit cells will of course take longer, although we will have fewer q-points to consider, alleviating some of the $O[N^3]$ increase due to the larger unit cell. One of our research goals will be to construct a “set-and-forget” mechanism which will search the Brillouin zone of an initial structure (here L1_0) find all unstable modes with supercells containing a given number of atoms, relax those modes, and repeat, until all such structures have been found. Even restricting ourselves to all possible binary intermetallics[1] this will require a Grand Challenge computational program.

6. Acknowledgments

M. J. Mehl is supported by the United States Office of Naval Research. Many of the computations reported here, including all of the VASP calculations, were performed at the Air Force Research Laboratory Department of Defense Supercomputing Resource Center, Wright-Patterson Air Force Base, Dayton OH, under a grant from the DoD High Performance Computing Modernization Program. The authors particularly wish to thank Prof. Harold Stokes for use of his ISOTROPY package.

References

- [1] S. Curtarolo, D. Morgan, K. Persson, J. Rodgers, G. Ceder, Predicting crystal structures with data mining of quantum calculations, *Phys. Rev. Lett.* 91 (13) (2003) 135503. doi:10.1103/PhysRevLett.91.135503. URL <http://link.aps.org/abstract/PRL/v91/e135503>
- [2] J. M. Sanchez, F. Ducastelle, D. Gratias, Generalized cluster description of multicomponent systems, *Physica A* 128 (1984) 334–350.
- [3] D. de Fontaine, Cluster approach to order-disorder transformations in alloys, *Solid State Physics* 47 (1994) 33–176.
- [4] A. Zunger, First-principles statistical mechanics of semiconductor alloys and intermetallic compounds, in: P. E. A. Turchi, A. Gonis (Eds.), *Statics and Dynamics of Alloy Phase Transitions*, NATO ASI Series, Ser. B, Plenum Press, New York, 1994, pp. 361–419.
- [5] A. van de Walle, G. Ceder, Automating first-principles phase diagram calculations, *Journal of Phase Equilibria* 23 (2002) 348.
- [6] D. Lerch, O. Wieckhorst, G. L. W. Hart, R. W. Forcade, S. Müller, Constructing cluster expansions for arbitrary lattices from minimal user input, *Model. Simul. Mater. Sci. Eng.* 17 (2009) 055003.
- [7] M. J. Mehl, D. A. Papaconstantopoulos, Applications of a tight-binding total-energy method for transition and noble metals: Elastic constants, *Phys. Rev. B* 54 (7) (1996) 4519–4530. doi:10.1103/PhysRevB.54.4519. URL <http://link.aps.org/abstract/PRB/v54/p4519>
- [8] H. Haas, C. Z. Wang, M. Fähnle, C. Elsässer, K. M. Ho, Environment-dependent tight-binding model for molybdenum, *Phys. Rev. B* 57 (3) (1998) 1461–1470. doi:10.1103/PhysRevB.57.1461. URL <http://link.aps.org/abstract/PRB/v57/p1461>
- [9] M. S. Daw, M. I. Baskes, Embedded-atom method: Derivation and application to impurities, surfaces, and other defects in metals, *Phys. Rev. B* 29 (12) (1984) 6443–6453. URL <http://link.aps.org/abstract/PRB/v29/p6443>

- [10] O. Levy, G. L. W. Hart, S. Curtarolo, Uncovering compounds by synergy of cluster expansion and high-throughput methods, *J. Am. Chem. Soc.* 132 (13) (2010) 4830–4833. doi:10.1021/ja9105623. URL <http://pubs.acs.org/doi/abs/10.1021/ja9105623>
- [11] G. L. W. Hart, R. Forcade, Generating derivative structures: Algorithm and applications, *Phys. Rev. B* 77 (2008) 224115.
- [12] G. L. W. Hart, R. Forcade, Generating derivative structures from multilattices: Application to hcp alloys, *Phys. Rev. B* 80 (2009) 014120.
- [13] B. C. Giessen, N. J. Grant, New intermediate phases in transition metal systems. ii, *J. Less-Common Metals* 18 (1965) 1080–1081. doi:10.1107/S0365110X65002566. URL <http://dx.doi.org/10.1107/S0365110X65002566>
- [14] B. C. Giessen, P. N. Dangel, N. J. Grant, New phases in the vanadium-iridium system and a tentative constitution diagram, *J. Less-Common Metals* 13 (1) (1967) 62–70. doi:10.1016/0022-5088(67)90047-1. URL [http://dx.doi.org/10.1016/0022-5088\(67\)90047-1](http://dx.doi.org/10.1016/0022-5088(67)90047-1)
- [15] R. M. Waterstrat, R. C. Manuszewski, The vanadium-rhodium constitution diagram, *J. Less-Common Metals* 52 (2) (1977) 293–305. doi:10.1016/0022-5088(77)90010-8. URL [http://dx.doi.org/10.1016/0022-5088\(77\)90010-8](http://dx.doi.org/10.1016/0022-5088(77)90010-8)
- [16] R. M. Waterstrat, B. Dickens, The crystal structure of v_3rh_5 , *J. Less-Common Metals* 31 (1) (1973) 61–67. doi:10.1016/0022-5088(73)90130-6. URL [http://dx.doi.org/10.1016/0022-5088\(73\)90130-6](http://dx.doi.org/10.1016/0022-5088(73)90130-6)
- [17] W. B. Pearson, *The Crystal Chemistry and Physics of Metals and Alloys*, Wiley-Interscience, New York, London, Sydney, Toronto, 1972.
- [18] B. Chen, H. F. Franzen, A second-order phase transition in $v_{0.54}ir_{0.46}$, *J. Less-Common Metals* 159 (1990) 343–347. doi:10.1016/0022-5088(90)90162-D. URL [http://dx.doi.org/10.1016/0022-5088\(90\)90162-D](http://dx.doi.org/10.1016/0022-5088(90)90162-D)

- [19] H. Baker (Ed.), Alloy Phase Diagram, ASM Handbooks Online, ASM International, 1991.
URL <http://www.asmmaterials.info/>
- [20] B. M. Klein, R. E. Cohen, Anharmonicity and the inverse isotope effect in the palladium-hydrogen system, *Phys. Rev. B* 45 (21) (1992) 12405–12414.
doi:10.1103/PhysRevB.45.12405.
URL <http://link.aps.org/abstract/PRB/v45/p12405>
- [21] S. Baroni, P. Giannozzi, A. Testa, Green's-function approach to linear response in solids, *Phys. Rev. Lett.* 58 (18) (1987) 1861–1864. doi:10.1103/PhysRevLett.58.1861.
URL <http://link.aps.org/doi/10.1103/PhysRevLett.58.1861>
- [22] S. Baroni, S. de Gironcoli, A. D. C. Adn Paolo Giannozzi, Phonons and related crystal properties from density-functional perturbation theory, *Rev. Mod. Phys.* 73 (2) (2001) 515–562.
doi:10.1103/RevModPhys.73.515.
URL <http://link.aps.org/doi/10.1103/RevModPhys.73.515>
- [23] X. Gonze, Adiabatic density-functional perturbation theory, *Phys. Rev. A* 52 (2) (1995) 1096–1114. doi:10.1103/PhysRevA.52.1096.
URL <http://link.aps.org/doi/10.1103/PhysRevA.52.1096>
- [24] S. Lee, R. Hoffmann, Bcc and fcc transition metals and alloys: A central role for the jahn-teller effect, *J. Am. Chem. Soc.* 124 (17) (2002) 4811–4823.
doi:10.1021/ja0114557.
URL <http://dx.doi.org/10.1021/ja0114557>
- [25] W. Kohn, L. J. Sham, Self-consistent equations including exchange and correlation effects, *Phys. Rev.* 140 (4A) (1965) A1133–A1138.
URL <http://link.aps.org/abstract/PR/v140/pA1133>
- [26] P. Hohenberg, W. Kohn, Inhomogeneous electron gas, *Phys. Rev.* 136 (3B) (1964) B864–B871.
URL <http://link.aps.org/abstract/PR/v136/pB864>
- [27] J. P. Perdew, K. Burke, M. Ernzerhof, Generalized gradient approximation made simple, *Phys. Rev. Lett.* 77 (18) (1996) 3865–3868.
URL <http://link.aps.org/abstract/PRL/v77/p3865>

- [28] G. Kresse, J. Hafner, *Ab initio* molecular dynamics for open-shell transition metals, Phys. Rev. B 48 (17) (1993) 13115–13118.
URL <http://link.aps.org/abstract/PRB/v48/p13115>
- [29] G. Kresse, J. Hafner, *Ab initio* molecular-dynamics simulation of the liquid-metal/amorphous- Phys. Rev. B 49 (20) (1994) 14251–14269.
URL <http://link.aps.org/abstract/PRB/v49/p14251>
- [30] G. Kresse, , Ph.D. thesis, Technische Universität Wien, Vienna (1993).
- [31] G. Kresse, D. Joubert, From ultrasoft pseudopotentials to the projector augmented-wave method Phys. Rev. B 59 (3) (1999) 1758–1775.
doi:10.1103/PhysRevB.59.1758.
URL <http://link.aps.org/abstract/PRB/v59/p1758>
- [32] P. Giannozzi, S. Baroni, N. Bonini, M. Calandra, R. Car, C. Cavazzoni, D. Ceresoli, G. L. Chiarotti, M. Cococcioni, I. Dabo, A. D. Corso, S. de Gironcoli, S. Fabris, G. Fratesi, R. Gebauer, U. Gerstmann, C. Gougoussis, A. Kokalj, M. Lazzeri, L. Martin-Samos, N. Marzari, F. Mauri, R. Mazzarello, S. Paolini, A. Pasquarello, L. Paulatto, C. Sbraccia, S. Scandolo, G. Sclauszero, A. P. Seitsonen, A. Smogunov, P. Umari, R. M. Wentzcovitch, Quantum espresso: a modular and open-source software project for quantum simulations of materials J. Phys.: Condens. Matt. 21 (39) (2009) 395502.
doi:10.1088/0953-8984/21/39/395502.
URL <http://iopscience.iop.org/0953-8984/21/39/395502/>
- [33] M. J. Gillan, Calculation of the vacancy formation energy in aluminium, J. Phys.: Condens. Matt. 1 (4) (1989) 689–711.
URL <http://stacks.iop.org/0953-8984/1/689>
- [34] H. T. Stokes, D. M. Hatch, B. J. Campbell, Isotropy, <http://stokes.byu.edu/isotropy.html> (2007).
- [35] B. J. Campbell, H. T. Stokes, D. E. Tanner, D. M. Hatch, Isodisplace: a web-based tool for exploring structural distortions, Journal of Applied Crystallography 39 (2006) 607–614.
- [36] S. C. Miller, W. F. Love, Tables of irreducible representations of space groups and co-representations of magnetic space groups, Pruett, Bolder, 1967.

- [37] C. Kittel, Introduction to Solid State Physics, 7th Edition, John Wiley & Sons, New York, 1996, Ch. 3, pp. 80–95.
- [38] M. Born, K. Huang, Dynamical Theory of Crystal Lattices, Oxford at the Clarendon Press, Oxford, 1966, Ch. 11-13.
- [39] K. Schubert, S. Bhan, W. Burkhardt, R. Gohle, H. G. Meissner, M. Pöttschke, E. Stolz, *Einige strukturelle Ergebnisse an metallischen Phasen (5)*, Naturwissenschaften 47 (13) (1960) 303. doi:10.1007/BF00600960. URL <http://dx.doi.org/10.1007/BF00600960>
- [40] P. Villars, L. D. Calvert (Eds.), Pearson's Handbook of Crystallographic Data for Intermetallic Phases, 2nd Edition, Vol. IV, ASM International, Materials Park, Ohio, 1991, p. 5091.